


Revealing channel polarization of atomic contacts of ferromagnets and strong paramagnets by shot-noise measurements

Martin W. Prestel , Marcel Strohmeier , Wolfgang Belzig , and Elke Scheer ^{*}
 Universität Konstanz, Fachbereich Physik, Universitätsstraße 10, 78464 Konstanz, Germany

 (Received 17 June 2021; revised 13 September 2021; accepted 14 September 2021; published 29 September 2021)

We report measurements of the shot noise of atomic contacts of the ferromagnets cobalt and gadolinium and the strong paramagnets palladium, platinum, and iridium. The contacts are fabricated using the mechanically controlled break-junction technique at 4 K. Single-atom contacts of Co and Gd with conductance smaller than the conductance quantum show reduced noise compared to the expectation for the spin-degenerate single-channel case. We discuss by how far this observation gives evidence for spin-polarized transport. Pd, Pt, and Ir reveal noise levels which are above, but close to the threshold to the spin-degenerate single-channel situation. Since for such multivalent metals more than one channel is expected to contribute to the transport, our findings do not exclude spin-polarized transport for these elements. We observe an anticorrelation between the minimum noise and the bulk Stoner parameter of these elements, supporting that spin polarization might be reflected in the shot-noise signal in strong paramagnets.

DOI: [10.1103/PhysRevB.104.115434](https://doi.org/10.1103/PhysRevB.104.115434)

I. INTRODUCTION

Since their first realization in the 1990s, atomic contacts serve as test-bed systems for exploring quantum-mechanical transport phenomena [1]. These include among others the electrical conductance, current-voltage characteristics, thermopower, shot noise, thermal transport, and spin-dependent transport and others [2]. In the quantum coherent regime these can be derived within the Landauer formalism which treats the transport as a wave scattering problem. For spin-degenerate systems the electrical conductance in the linear-response regime corresponds to the total quantum-mechanical transmission multiplied by the conductance quantum $G_0 = \frac{2e^2}{h}$,

$$G = G_0 \sum_i \tau_i, \quad (1)$$

where τ_i 's are the transmission coefficients and the number i of the spin-degenerate channels is related to the chemical valence of the metal [1]. When the spin degeneracy is lifted, the channels corresponding to the two spin directions, may differ in terms of number and transmission coefficients. The Landauer formula for the linear conductance then reads

$$G = G_{\uparrow} + G_{\downarrow} = \frac{G_0}{2} \sum_{i,\sigma} \tau_{i,\sigma}, \quad (2)$$

with $\sigma = \uparrow, \downarrow$ denoting the two spin directions. One possibility that has been suggested to reveal a possible influence of the spin onto the transport are shot-noise measurements. In 1918 Schottky discovered a noise in vacuum diodes arising from the discrete nature of electrons $S_I = 2e|I|$ [3] with the average current $|I|$. Here, the current noise power is defined as $S_I = 2 \int dt \langle I(t)I(0) \rangle$, where $\langle \dots \rangle$ denotes a quantum-

mechanical average. In the framework of the Landauer picture this so-called quantum shot noise depends on the transmission coefficients. For a finite temperature T and an applied bias voltage V the noise power is given by Ref. [4] (k_B denotes the Boltzmann constant),

$$S_I = eV G_0 \coth \left(\frac{eV}{2k_B T} \right) \sum_{i,\sigma} \tau_{i,\sigma} (1 - \tau_{i,\sigma}) + 2k_B T G_0 \sum_{i,\sigma} \tau_{i,\sigma}^2. \quad (3)$$

The reduction compared to the full shot noise of $S_I = 2e|I|$ is often expressed by the so-called Fano factor [5], which can be calculated from the transmission channels via

$$F = \frac{\sum_{i,\sigma} \tau_{i,\sigma} (1 - \tau_{i,\sigma})}{\sum_{i,\sigma} \tau_{i,\sigma}}. \quad (4)$$

Figure 1 shows the expected minimum noise for contacts in which the transmission channels open one by one when increasing the conductance for the spin-degenerate case (solid line) and for different values of the spin polarization (dotted lines) where the spin polarization is defined as

$$P = \frac{G_{\uparrow} - G_{\downarrow}}{G_{\uparrow} + G_{\downarrow}}. \quad (5)$$

The area shaded in gray between the dashed and the solid line indicates spin-polarized transport, the one shaded in rose, below the dashed line, cannot be reached within this model. Note that for incomplete opening of the channels, i.e., if the transmission coefficients do not reach the value $\tau_{i,\sigma} = 1$ before the next channel starts to contribute, the noise is always higher than the respective threshold lines. First measurements of this reduction in atomic contacts have been reported by van den Brom and van Ruitenbeek [6] for the monovalent nonmagnetic metal Au showing a characteristic decrease in

^{*}Corresponding author: elke.scheer@uni-konstanz.de

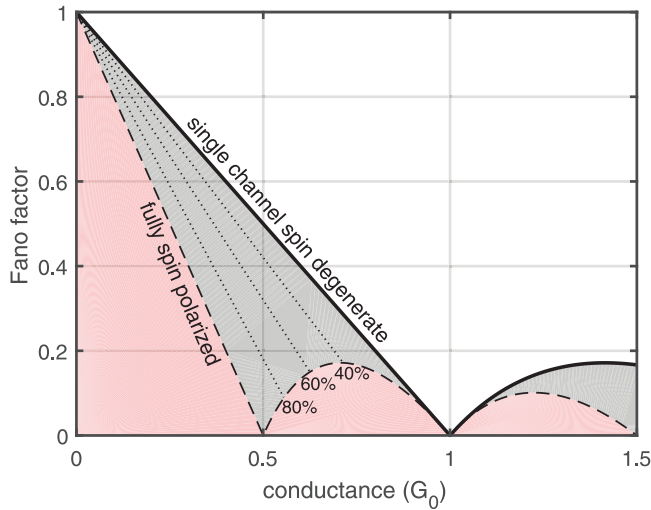


FIG. 1. The reduction of the shot noise compared to the full shot-noise $2e|I|$ is expressed by the Fano factor. Minimal lines for single-channel spin-degenerate (bold) and fully spin-polarized (dash-dotted) transport are shown. The gray area is only allowed for spin-polarized transport. Different degrees of spin polarization for one spin-up and one spin-down channel are displayed with dotted lines.

noise around integer multiples of the conductance quantum: $G \simeq nG_0$, confirming the expected full saturation of the transmission coefficients.

However, a similar reduction of the Fano factor is expected for every kind of symmetry breaking, which lifts the degeneracy and can, hence, be regarded as effective channel polarization as we will discuss next. We consider a contact described by a certain number N of channels with a set of transmission coefficients $\{\tau_n\}$. The goal is to relate the channel distribution to observable quantities. In the following we set $G_0/2 = e^2/h = 1$ and count spin as just another channel index. We express the Fano factor $F = [\sum_n \tau_n(1 - \tau_n)]/(\sum_n \tau_n)$ in terms of the average transmission $\bar{\tau} = (1/N) \sum_n \tau_n$, the conductance $G = N\bar{\tau}$, and the channel variance $\delta\tau^2 = (1/N) \sum_n (\tau_n - \bar{\tau})^2$. This yields

$$F = 1 - \bar{\tau} - \frac{\delta\tau^2}{\bar{\tau}} = 1 - \frac{G}{N} - \frac{N}{G}\delta\tau^2. \quad (6)$$

This equation shows that increasing the channel variance reduces the Fano factor at a fixed average transmission.

We can now relate the average transmission to the channel variance for a fixed Fano factor. Solving for $\bar{\tau}$ we obtain

$$\frac{\bar{\tau}}{1 - F} = \frac{G}{N(1 - F)} = \frac{1}{2} \left[1 \pm \sqrt{1 - \frac{4\delta\tau^2}{(1 - F)^2}} \right]. \quad (7)$$

For the experimental systems studied here, mainly the + sign seems to be important since for most contacts $G > N(1 - F)/2$. Note that the argument of the square root is always positive and, hence, the channel variance and the Fano factor are related by the inequality $\delta\tau < (1 - F)/2$. This aspect becomes, in particular, important when studying contacts with

more than two “orbital channels,” i.e. more than four spin-resolved channels. If one observes a reduced Fano factor compared to the fully degenerate case with identical τ_n for all channels, it cannot be decided if the reduction of F arises from lifting the spin degeneracy or the orbital degeneracy. In other words, a conclusion about spin polarization can only be drawn for contacts with at most two channels. We will come back to this aspect when interpreting our observations for atomic contacts of the strong paramagnets below.

However, since transport through ferromagnetic materials is expected to be spin polarized, we will assume for these that if a reduction of the Fano factor is observed, the underlying channel polarization is indeed the spin polarization of the conduction electrons. For bulk Co, for example, a spin polarization of roughly 40% is expected [7,8]. Further evidence for spin-polarized transport in atomic contacts of Co fabricated by the mechanically controlled break junction (MCBJ) technique can be concluded from magnetoresistance measurements [9] and from scanning tunneling spectroscopy revealing signatures of the Kondo effect [10]. The contacts in these two studies have in common that both electrodes as well as the contacts are formed by Co. From shot-noise measurements in single-atom contacts formed by individual Co atoms adsorbed on a nonmagnetic Au(111) surface and assuming a single spin-up and a single spin-down channel, Burtzclaff *et al.* found a value of 50% [11] as well. So far only few works have experimentally addressed the shot-noise single-atom contacts of a ferromagnetic element with ferromagnetic electrodes [12,13]. Reference [12] mainly concentrates on the formation of atomic chains by the incorporation of molecules but does not report indications of spin polarization for the pure metallic contacts. In Ref. [13] atomic contacts of Fe, Ni, and Co in comparison with Cu were investigated using a similar MCBJ technique as applied here. In their experiments no data points below the threshold line for spin-polarized transport was found, but instead enhanced Fano factors of the ferromagnetic contacts compared to the noble-metal Cu were observed. These findings were rationalized with the help of simulations by the contribution of the d orbitals to the transport. For bulk strong paramagnets, such as Pt, Pd, or Ir, no spin polarization is expected. However, recently Strigl and co-workers [14,15] and Prestel *et al.* [16] reported evidence for local magnetic ordering in atomic contacts of these metals as it was theoretically predicted for such contacts [17–20]. Hence, one may also expect spin-polarized transport in atomic contacts of these metals. With the help of shot-noise measurements, Kumar *et al.* [21] searched for indications of spin polarization in atomic contacts of Pt but found only a clustering of data points at the border to spin-polarized transport for systems showing channel saturation. (i.e., above, but close to the solid line in Fig. 1). However, since in single-atom contacts of the transition-metal Pt with a total conductance between 1.6 and $1.8G_0$, at least, five spin-resolved channels [21] have to contribute to the transport, their findings would still be in agreement with partially opened spin-polarized channels. Assuming spin degenerate transport, Pauly *et al.* [22] calculated three spin-degenerate channels (i.e., six spin-resolved channels) for single-atom Pt contacts. Furthermore, from a theoretical analysis, the authors of Ref. [21] concluded that although atomic contacts are expected to be magnetically

ordered, this order is not necessarily reflected by a spin polarization of the transport channels, e.g., if the magnetic order is formed by partially occupied d orbitals and the transport is dominated by s orbitals. In the present paper we follow the approach from Ref. [21], but in addition we strive to explore the conductance range below $1G_0$ where a lower number of contributing channels is expected, and so the chance to find clear evidence for spin polarization is higher.

II. EXPERIMENTAL METHODS

A. Sample fabrication

For fabricating atomic contacts we use the MCBJ technique [23], see the Appendix for more information. The samples are produced on a nonmagnetic phosphor bronze (thickness 200 μm) covered with a thin layer (~ 1.5 μm thickness) of polyimide (PI). For Co, Gd, and Pd a simple liftoff process is used as described, e.g., in Ref. [15]. To this end the substrate is covered with a double layer of electron-beam resist (MMA-MAA EL11 and polymethylmethacrylate from Microchemicals), cut into small pieces (18×3 mm^2) and patterned in a scanning electron microscope. After development, the desired metal is evaporated onto the chip. For Co and Pd the desired thickness is around 80 nm. Due to fast oxidation of Gd the thickness is enhanced to, at least, 150 nm. For Pt and Ir a subtractive patterning described in Strigl *et al.* [14] and Prestel *et al.* [16] is applied. Here, first a 80-nm-thick layer of the desired metal is sputtered onto the PI. This film is then structured using an electron-beam defined Al mask and a SF_6 plasma. All samples are underetched in an O_2 plasma to form freestanding bridges over a length of 1 to 2 μm . The resistance at room temperature before cool down is around 100 Ω for Ir, Pd, and Pt and around 1 k Ω for Co and Gd. After cool down to 4.2 K a soft electromigration is applied to purify the metal in the constriction [24].

B. Transport measurements

In this paper we use a low-noise current-voltage converter by Janásek [25] to measure the noise in the sample. To avoid any avoidable additional noise sources in the setup a simple two-point configuration is used. The sample is biased through an active low-pass filter (lp) with a cutoff frequency of 16 Hz. The wiring inside the cryostat is home built and features a resistance of 10 Ω and a capacitance of about 100 pF in the cold state. A schematics of the circuit is depicted in Fig. 2(a) including all noise sources present in the setup. The low-pass filter, the wiring, and the current-voltage converter add a voltage noise W_u to the setup. The additional current noise of the current-voltage converter W_i^{amp} can be measured separately and subtracted from the signal. To obtain the real physical noise out of the measured noise contributions, the influence of the impedance of the setup has to be taken into account as described in the next section.

The setup is designed to measure the shot noise directly using a current amplifier instead of measuring the voltage signal and calculating the current noise from this signal. The same approach was already used by Karimi *et al.* [26], but here we present a setup with a much higher frequency range up to 800 kHz. The maximum frequency is limited by the

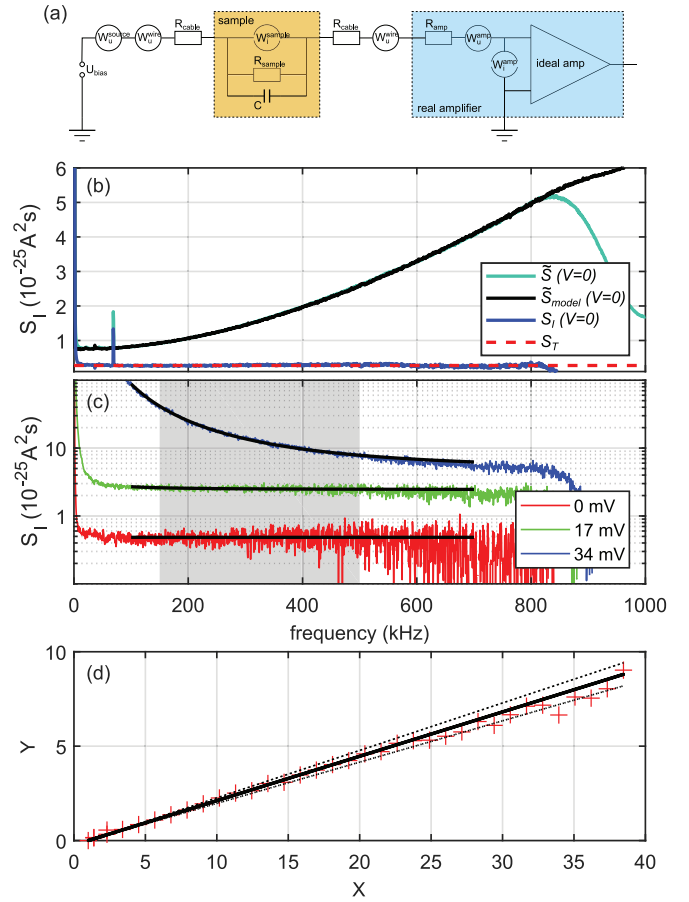


FIG. 2. The data evaluation from the raw spectra to the Fano factor: (a) Measurement circuit. (b) Measured \tilde{S} (cyan) and modeled \tilde{S}_{model} zero-bias spectrum of a contact are shown. \tilde{S}_{model} is used to calculate the corrections required to obtain the sample noise $S_I(V=0)$ (blue) which in case of $V=0$ equals the thermal noise S_T (red, dashed). (c) Zero-bias and two examples of finite-bias spectra of the contact shown in (b) together with fits (black lines) to the data according to Eq. (9). (d) Normalized presentation [see Eq. (10)] of the shot noise data (red symbols) used to determine the Fano factor (slope of the black line) and its uncertainty (dotted lines).

combination of the current-voltage converter and the oscilloscope (NI PXIe-5922) operated such that aliasing effects are avoided. Each spectrum is built up by averaging over 1000 spectra each obtained by fast Fourier transformation of the time-based data measured by the oscilloscope card.

C. Data evaluation

A contact is adjusted by moving the tips of the MCBJ by bending the substrate. If a contact in the atomic regime with a resistance of 4–50 k Ω is formed, the movement is stopped, and the contact is allowed to thermalize for 1 min. An IV curve is recorded before and after a series of noise spectra is taken at different bias voltages. The first and the last spectra are always recorded at zero voltage. If the IV and zero-bias spectra at the beginning and the end differ from each other, the respective contact is not analyzed further. For a stable contact the IV curves reveal the sample resistance R_{sample} .

To obtain the intrinsic sample noise S_I from the measured noise signal \tilde{S} we use the two zero-bias spectra and correct for the current W_i^{amp} and voltage noise ($W_u^{\text{amp}}, W_u^{\text{lp}}$) contributions of the amplifiers and the circuit. The correction depend on the frequency f and the capacitance C . Based on the circuit in Fig. 2(a), \tilde{S} can be modeled as

$$\tilde{S} = S_I \left[\frac{Z}{Z + R_s} \right]^2 + W_i^{\text{amp}} + \frac{W_u^{\text{amp}} + W_u^{\text{lp}}}{|Z + R_s|^2}, \quad (8)$$

where $Z = (i\omega C + 1/R_{\text{sample}})^{-1}$ is the impedance and R_s the total series resistance of the setup. In the zero-bias limit S_I is simply given by the thermal noise $S_T = 4k_B T/R$. With the knowledge of the temperature T and the capacitance C the measured zero-bias noise $\tilde{S}(V=0)$ can be fitted with Eq. (8). $S_I(V=0)$ can then be calculated. This correction has to be performed for each contact separately. In Fig. 2(b) the measured $\tilde{S}(V=0)$ (cyan) and the modeled zero-bias spectrum $\tilde{S}_{\text{model}}(V=0)$ are exemplified for one particular contact. The model follows the measured data up to a frequency of about 800 kHz. Here the cutoff frequency of the oscilloscope imposes an upper limit which is not considered in Eq. (8). The blue curve depicts the resulting sample noise $S_I(V=0)$. For comparison the thermal noise $S_T = 4k_B T/R$ (red) is also shown. Applying this correction procedure to all other spectra $\tilde{S}(V)$ of one contact leads to fairly white spectra for low bias, see Fig. 2(c). The usual flicker noise $1/f^\alpha$ contribution is observed, which emerges with increasing bias and which is attributed, among others, to two-level fluctuations in the leads [27]. To extract, in particular, the white-noise part of the measurements an analysis similar to Mu *et al.* [27] is applied. A power function,

$$S_I(f) = (a/f)^\alpha + b \quad (9)$$

is used to fit the $1/f^\alpha$ trend of the spectra. By performing this we consider the constant term $S_w(V) := b [A^2 s]$ further as the white noise, i.e., the thermal noise plus the shot noise of the contact. Selected spectra $S_I(V)$ as well as the fit and the constant white noise are shown in Fig. 2(c). The white-noise part is used to calculate the normalized noise $Y = \frac{S_I(V) - S_I(0)}{S_I(0)}$ and the normalized voltage $X = x \coth x$ with $x = eV/2k_B T$, following Ref. [5]. A linear fit,

$$Y = F(X - 1), \quad (10)$$

to this data returns the Fano factor F . The indicated uncertainty of F corresponds to the fit uncertainty. The normalized noise Y as a function of the normalized voltage X is shown together with the fit and uncertainties in Fig. 2(d).

Atomic contacts of Au serve as test bed for the setup and the data evaluation since their noise properties are well characterized and understood. Au single-atom contacts feature dominantly single-channel transport with a minor second channel [6,28,29]. We also find Fano factors, which mainly coincide with the theoretical line for single-channel transport (cf. Fig. 3). Contacts with conductance above $1G_0$ and $2G_0$, respectively, show a higher spread of Fano factors with an average well above the theoretically possible minimal noise limit. We attribute this enhanced noise to two reasons.

First, the number of data points is low because of the difficulty to establish stable contacts in these conductance ranges.

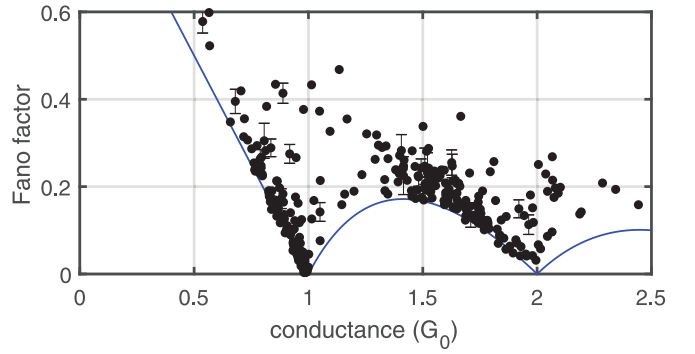


FIG. 3. Shot noise in atomic contacts made of Au, showing mostly single-channel transport. The error bars are only shown if the uncertainty is larger than the symbol size.

Second, the theoretical limit assumes that the first channels saturate before the subsequent are opening. In addition these contacts are necessarily disordered contact. Disorder leads to only partially opened channels causing higher Fano factors [6].

III. RESULTS AND DISCUSSION

A. Ferromagnets

Figure 4 shows the experimental data of the present paper for Co, in the same representation as Fig. 1. We observe a clustering of Fano factors well above the solid black line for most of the contacts (gray data points). For contacts with small conductance below $1G_0$ we also find Fano factors below the black line; these data points are highlighted in black, although for

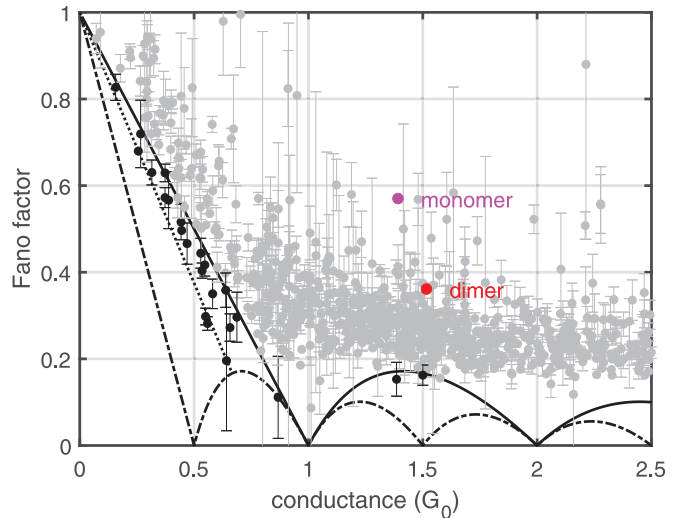


FIG. 4. Shot noise in Co atomic contacts, showing the spin polarization for contacts below $1G_0$ of up to 50%. The dotted line marks 50% spin polarization. From the gray data points no spin polarization can be determined within the independent channel model, and the black ones are indicative for spin polarization. For clarity the error bars are shown only if the error exceeds the symbol size. The magenta and red data points are calculated values for the conductance and the Fano factor for a monomer and a dimer using the transmissions given in Ref. [8].

some of them the error bars expand beyond the threshold line. We, thus, confirm the observation of Ref. [11] of roughly 50% spin polarization for contacts below $1G_0$. From conductance histograms (see the Appendix) and earlier reports it is known that the preferred conductance of Co single-atom contacts between Co electrodes amounts to about $1.5G_0$ [8,9]. We, therefore, attribute the contacts with $G < 1G_0$ to disordered or even close-to-tunneling contacts in which the single-channel model is applicable [1].

Furthermore, we also found occasionally data points at the borderline to the spin-polarized area for contacts around $1.5G_0$ in Co. Calculations by Häfner *et al.* for model single-atom contacts, forming either a short contact (monomer) or a short wire (dimer) between bulk Co electrodes, predict a conductance of $1.5G_0$ ($1.6G_0$) and a spin polarization of -13% (-42%) for the monomer (dimer), respectively. The two configurations have three spin-up channels each and eight (six) spin-down channels with different contributions to the transport [8]. Furthermore, the authors estimated the influence of disorder and found that the number of channels is robust with respect to disorder, whereas the spin polarization of the monomers may change sign and its average is close to zero. For the dimers the distribution of the spin polarization is centered around -40% . Using the transmission coefficients calculated for the ideal monomer and dimer structures we calculated their expected Fano factors and plotted them in Fig. 4 in magenta and red. These two data points are well above the black solid line for the spin-degenerate single-channel case but also above the majority of the experimental data points, suggesting that also the experimentally studied contacts may host spin-polarized channels. The fact that the experimental Fano factors are smaller than the calculated ones for idealized geometries [8] can be naturally explained by disorder, lifting the orbital spin degeneracy. Summarizing the findings on Co, we conclude that many contacts, the Fano factors of which are not below the single-channel spin-degenerate line, also show a trend towards lower F which might be indicative for spin polarization. For more than two channels it is not possible to determine the degree of spin polarization from the Fano factor solely. Even an exact analysis of the channel distribution [6] would not allow for a statement of the spin polarization for a single contact since only the value but not the spin direction can be extracted. Vardimon *et al.* presented a possibility to extract borders for the number and transmission coefficients of channels from a statistical analysis of the noise distribution of thousands of contacts for up to four spin-degenerate channels [30]. In view of the large number of channels in Co contacts, such an analysis is not possible here.

Whereas Co can be assigned to the $3d$ ferromagnetic materials, Gd is, in particular, characterized by its partially filled $4f$ shell leading to an electronic configuration of $[\text{Xe}] 4f^7 5d^1 6s^2$. As expected for lanthanide metals, magnetism is mainly driven by $4f$ moments with local and insulating characters. Conductance, however, can be mainly associated to delocalized s and d valence bands. Experimental and theoretical studies on bulk Gd have shown that the conduction-electron moment is on the order of $0.63\mu_B$ and gives, therefore, a rather small contribution to the total moment of $7.63\mu_B$ [31,32]. Reducing the physical dimensions of the subject is commonly linked to a change in the density

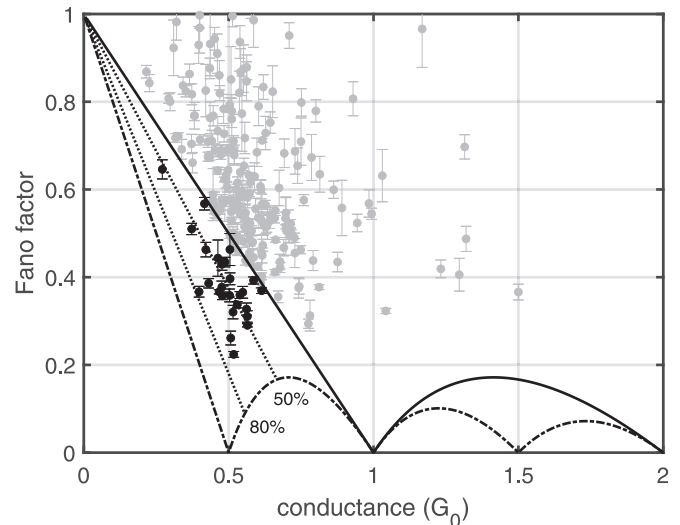


FIG. 5. Shot noise in atomic Gd contacts, showing the spin polarization for contacts below $1G_0$. In particular a clustering of the data points is observed that might indicate a tendency for spin polarization towards the 50% limit. The noise measurement is limited to the regime of the single-atom contact, the conductance peak of which was measured between 0.5 and $0.8G_0$.

of states (DOS) and exchange interactions. Thus, atomic size contacts of Gd can be seen as an interesting model system for quantum transport in the presence of strong local magnetism. Experimentally only conductance histograms have been measured so far using the MCBJ technique as well as scanning tunneling microscopy point contact studies [33,34]. Further insights on the electronic structure and transport behavior are given by density functional theory (DFT) calculations from Olivera *et al.* [33]. By comparing the bulk material with one-dimensional nanocontacts they predict a strong change in the spin-resolved DOS associated with the reduced dimensions. An increase in the total magnetic moment up to $8.9\mu_B$ is explained by an additional polarization of the d bands. As a considerable large $d-d$ exchange coupling clearly favors the ferromagnetic configuration, one may ask if the electronic transport is affected by these observations. A shift in the spin-resolved DOS at the Fermi energy which involves conducting electrons should give rise to a spin polarization of current through atomic Gd contacts.

Figure 5 summarizes the results from shot-noise measurements on two different Gd samples, based on the contacts which a linear $Y(X)$ relation as exemplified in Figs. 6(a) and 6(b). Both samples are comparable regarding their statistical distribution of data points in the $F(G)$ space. In agreement with previous studies [33,34] we found a conductance peak of the one atom contact which is on the order of $0.5-0.8G_0$ [see Fig. 8(c)] in the Appendix). Therefore, the noise measurement is limited to the conductance regime below $1G_0$ where less channels are expected to be involved in transmission. The vast majority of data points in Fig. 5 is above the threshold for spin-polarized transport for a single-channel situation. However, roughly 10% of the evaluated contacts can be assigned to a clearly spin-polarized transport behavior. Here we observe a clustering of the data points that might

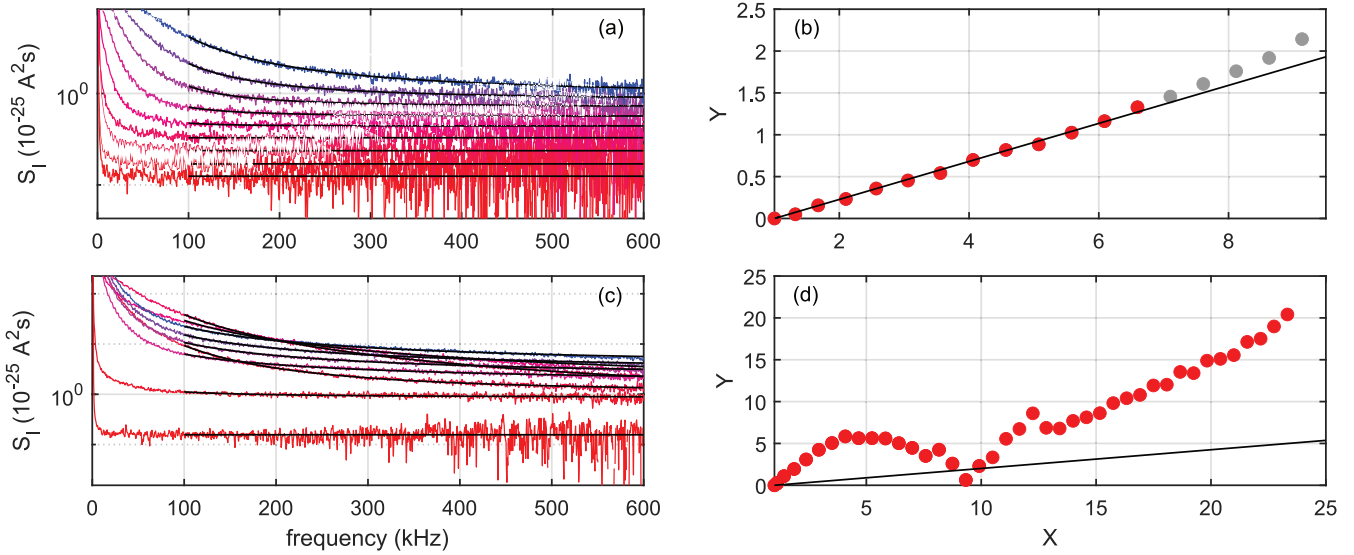


FIG. 6. Exemplary shot-noise measurements on two Gd atomic contacts. (a) Selected spectra measured on a spin-polarized contact with conductance $G = 0.52G_0$ (colored lines: experimental data, black: fits to the data) for applied voltages $V \in \{0, 2.5, 5, 7.5, 10, 12.5, 15, 17.5, 20\}$ mV from red to blue. (b) Selected $X(Y)$ data point for the contact shown in (a). Our data evaluation yields a Fano factor of $F = 0.22$, which corresponds to the smallest Fano factor in Fig. 5. Grey data points above $X = 7$ do not contribute to the determination of F by linear regression based on the relation $Y = F(X - 1)$ (black line). (c) Same as in (a) but for a contact that shows additional noise contributions with strong $1/f^\alpha$ -like character and with non-monotonic dependence on the applied voltage. (d) Same as (b) but for the contact shown in (c). A meaningful determination of F is not possible. Also the black line is the same as in (b) as guide to the eye.

indicate a tendency of the spin polarization around 50%. Also this result supports previous calculations reported by Olivera *et al.* [33]. According to their DFT studies on pyramidal atomic contacts a spin polarization up to 70% can be derived from the spin-resolved conductance characteristics. Thereby the polarization varies sensitively depending on the contact geometry (dimer or monomer) as well as on the distance between both apex atoms. An explanation was given by the variety of involved eigenchannels in Gd nanocontacts. Overall, it was shown that predominantly s , p_z as well as hybrid sp_z orbitals contribute to the polarized transport. A significant contribution of polarized d states could be observed in stretched monomer configuration. Regarding the Fano factor, it is, therefore, not expected that the corresponding data points in the $F(X)$ plot even for spin-polarized contacts will be below the conventional spin-degenerate threshold line.

It is worth mentioning that only 5% of the investigated Gd contacts showed a linear relation between the current and the current noise in the frequency range accessible to our measurement. An example is given in Figs. 6(a) and 6(b) which illustrates that these kinds of contacts show a small and monotonously rising excess noise upon increasing the voltage up to about $X = 6$ to 12, depending on the contact. All data presented in Fig. 5 have been obtained from these contacts. The remaining 95% of contacts showed an additional noise contribution with much stronger $(1/f^\alpha)$ -like character and with nonmonotonous dependence on the applied voltage as shown in Figs. 6(c) and 6(d). Treating the data, nevertheless, with the data evaluation scheme presented above, resulting in the fits [black lines in Fig. 6(d)] leads to a nonlinear appearance of the remaining signal in the $Y(X)$ characteristics. It should be noted, that the contact shown here is only representative with respect to the appearance of

the additional noise, but not in its exact voltage dependency. Please note that the Y axis of Fig. 6(d) is a factor of 10 larger than the one in Fig. 6(b), i.e., the overall noise level, also the frequency independent part, is markedly enhanced compared to the contact shown in Fig. 6(b). The observed reduction of the noise in Fig. 6(d) around $X = 9.3$ to $Y \approx 0.6$ would correspond to $F \approx 0.08$ as indicated by the black line in Fig. 6(d), which would be compatible with the behavior of the “regular” contacts shown in Figs. 6(a) and 6(b). Based on this phenomenology, we tentatively attribute the enhanced noise contributions below and above the minimum to two-level fluctuations caused by different fluctuators activated in the respective voltage regimes. Depending on the exact contact geometry there might be a specific voltage range where fluctuations are favored or suppressed. We note that the data shown are just one example of this nontrivial behavior and cannot be considered as typical. The development of a detailed analysis of this behavior is beyond the scope of the present article. For gold contacts under very high bias a correlation between the shape of the IV ’s and a nonlinear bias dependence of the shot noise at much higher bias had been found and attribute to quantum interference phenomena in the leads [35]. To test this aspect for the Gd contacts investigated here, we show in the Appendix in Fig. 9 the corresponding IV ’s of the contacts of Fig. 6 in the bias range of -30 to 30 mV where we observe only small nonlinearities symmetrically around zero bias for both contacts. Based on this comparison we cannot conclude if the same mechanism would be at play here.

B. Strong paramagnets

The measurements on strong paramagnets are shown together in Fig. 7. The insets show the $F(G)$ plots for each

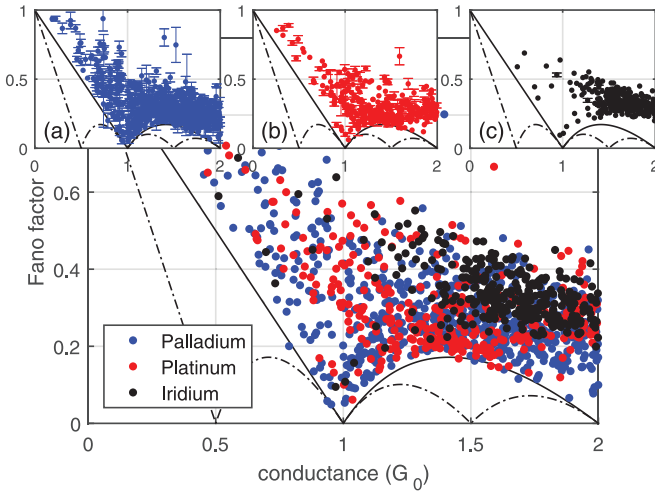


FIG. 7. Comparison of the three strong paramagnets Pd, Pt, and Ir. The data for the each metal are presented separately in the insets in the top of the figure. The error bars are only shown if bigger than the symbol size. The gap between the single-channel spin-degenerate line and the data points increase from Pd over Pt to Ir.

metal, Pd, Pt, and Ir separately, with error bars if the uncertainty is bigger than the symbol size. For Pd and Pt a clustering of data points at the single-channel line for spin-degenerate transport in the atomic contact regime ($1.5G_0$) is present, comparable with the results reported by Kumar *et al.*, who had concentrated their investigations on this conductance range for Pt solely [21]. For contacts with smaller conductance $0.5G_0 < G < 1G_0$ we observe for Pd also a clustering at the single-channel line, whereas for Pt the Fano factor is clearly higher. For Ir the data points are clearly above the spin-degenerate line over the whole investigated conductance range.

In view of the results of Co and the fact that also for single-atom contacts of Pt, Pd, and Ir more than a single orbital channel per spin direction are expected, a spin polarization in atomic contacts of strong paramagnets can neither be excluded nor supported. However, assuming similar geometrical disorder, we interpret our observations based on the paramagnetic properties of the bulk metals.

Although the channel distribution is not known in detail, we can assume that statistically for a fixed conductance, a lower Fano factor would correspond to higher channel polarization. Thus, the closer the data points are located to the single-channel threshold line, the higher would be the polarization. Comparing the three elements under study here, we observe an increasing distance to the single-channel line for spin-degenerate transport from Pd over Pt to Ir. This trend correlates with the Stoner enhancement $I = \frac{1}{2}UD(E_F)$ [36] for these three metals with U as the Stoner parameter and $D(E_F)$ as the DOS at the Fermi energy. The values are given in Table I with the largest value for Pd and the smallest for Ir. In the light of our considerations expressed in Eqs. (6) and (7) we cannot directly relate the observed reduction of the Fano factor to the spin polarization, but any degeneracy lifting would have a similar effect. Hence, we make the bold

TABLE I. The Stoner enhancement I for the three strong paramagnets Pd, Pt, and Ir. The values have been calculated from the parameters given in Refs. [37–39].

	Palladium	Platinum	Iridium
$I = \frac{1}{2}UD(E_F)$	0.775–0.86	0.57	0.27

assumption that any possible lifted channel degeneracy is affected by the Stoner enhancement. Considering the effect on some channel that without interaction would be degenerate we conclude that the transmission of this channel can be expressed as $\tau_n = \bar{\tau}_n \pm I\delta\tau_n$. The effect of this particular lifting of degeneracy increases the channel variance by $\Delta\tau_n^2 = \frac{1}{2}[(\tau + I\delta\tau)^2 + (\tau - I\delta\tau)^2 - 2\tau^2] = I^2\delta\tau_n^2$. Hence, we conclude that any interaction-induced lifting of a degeneracy results in a reduction of the Fano factor. This is in agreement with the trend observed experimentally.

IV. CONCLUSION

In this paper, we presented an experimental study of the shot noise in atomic contacts of the band ferromagnet Co, the rare-earth ferromagnet Gd, and the strong paramagnets Pd, Pt, and Ir at low temperatures. Since these metals are multivalent several orbital channels are expected to contribute also to the transport in single-atom contacts. We show that under these conditions measurements of the shot noise cannot distinguish between lifting spin degeneracy or breaking another symmetry, e.g., by a disordered atomic configuration. In our experiment, the contacts are arranged by stretching nanobridges of the (homogeneous) materials. We use an electronic setup that allows the analysis of data up to 600 kHz to be able to measure also at high bias in a frequency range beyond the influence of $1/f^\alpha$ noise. Contributions to the total noise signal are accounted for by a transfer function, modeling the electric setup quantitatively as confirmed by control experiments on the well-studied system of Au atomic contacts. For Co we found shot-noise amplitudes, quantified by the Fano factor as expected for spin-polarized transport in agreement with earlier measurements on individual Co using spin-degenerate electrode material. For Gd we find two different behaviors. The one class of contacts shows a linear dependence of the shot noise on the transport voltage with a Fano factor corresponding to spin-polarized transport, although the $4f$ -orbitals which are responsible for the magnetic ordering in Gd do not contribute directly to the conduction channels. A larger fraction of contacts shows a nonuniform dependence of both the $1/f^\alpha$ noise and the shot noise on the transport voltage, revealing the complex magnetic properties of the lanthanides. Finally, for the strong paramagnets we observe Fano factors which are compatible with both spin-degenerate and spin-polarized transport for atomic contacts of multivalent metals. We discuss to what extent the Fano factor is indeed indicative for spin-polarization, since also any other degeneracy lifting would have a similar effect onto the Fano factor. We observe a correlation between the Stoner factor and the Fano factor of the strong paramagnets: Ir which according to the Stoner criterion is the “weakest” among the strong

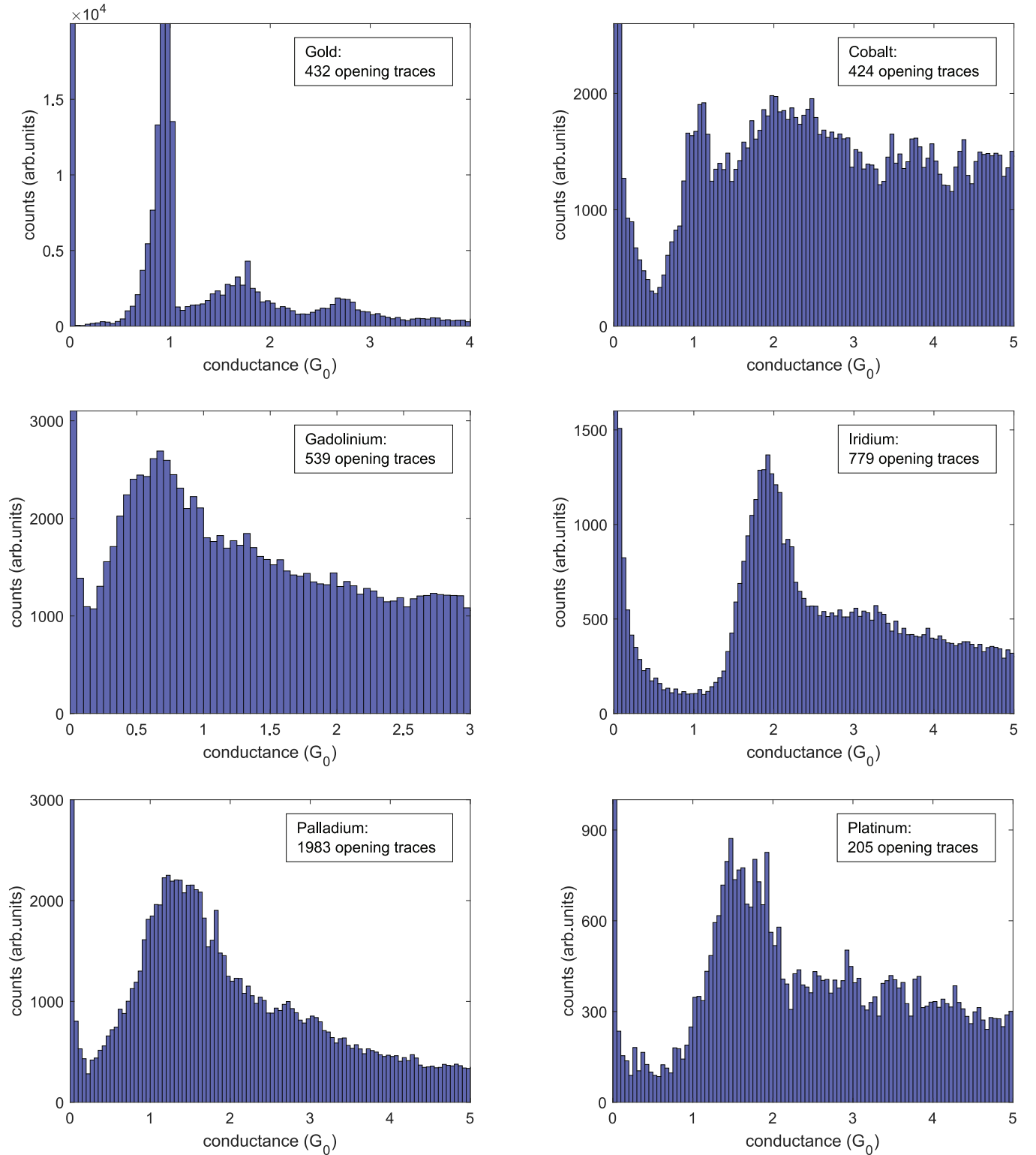


FIG. 8. Representative conductance histograms for the elements Au, Co, Gd, Ir, Pd, and Pt. All measurements were constructed from several hundred opening curves recorded under cryogenic conditions at 4.2 K.

paramagnets shows Fano factors well above the threshold for twofold degenerate single-channel contacts. This does, however, not exclude spin-polarized transport, since multivalent metals with several, not saturated transport channels are expected to have higher Fano factors. In comparison, Pt

with a somewhat bigger Stoner parameter, reveals smaller Fano factors for contacts with the same conductance as Ir. Interestingly for Pd, the metal with the largest Stoner parameter, the minimum Fano factors follow the threshold line for the single-channel case, a finding that is not expected for

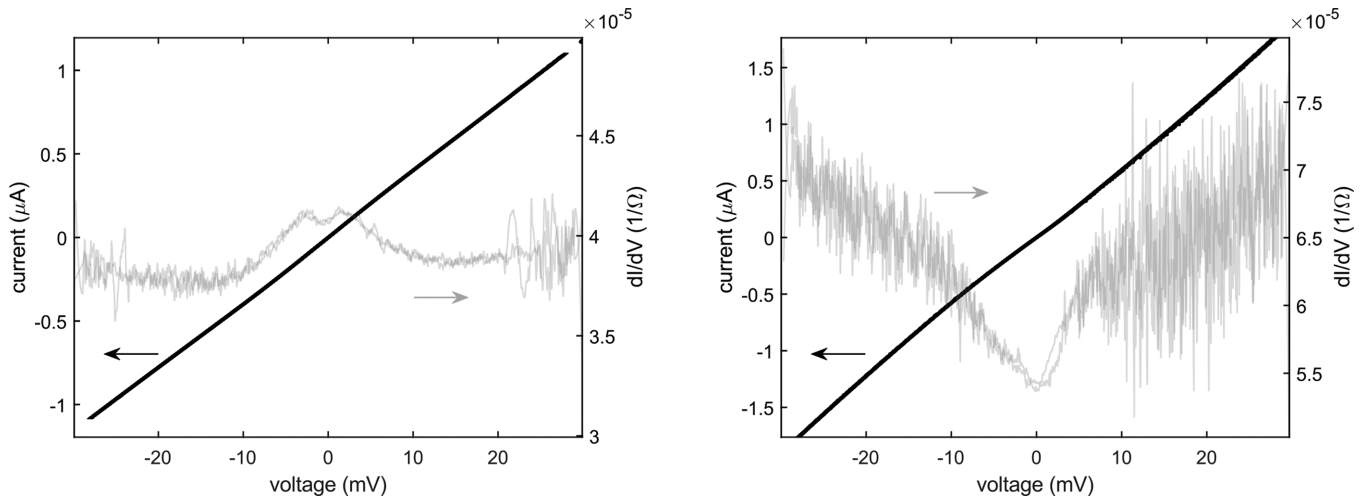


FIG. 9. Current-voltage characteristics (black) and their numerical derivative dI/dV (gray) for both contacts of which the noise properties are presented in Fig. 6 of the main article. The left curves correspond to the regular contact in Figs. 6(a) and 6(b) whereas the IV on the right can be linked to Figs. 6(c) and 6(d).

multivalent elements. This observation needs further theoretical investigation.

ACKNOWLEDGMENTS

We thank T. B. Möller and A. Di Bernardo for fruitful discussion and A. Fischer, M. Hagner, S. Haus, J. Maier, and R. Sieber for technical support. We acknowledge funding by the Deutsche Forschungsgemeinschaft (DFG, German Research Foundation)—Sche505/12 - Project No. 262725753 and SFB1432 - Project No. 425217212 as well as by the Carl-Zeiss Foundation through an individual fellowship for M.W.P.

APPENDIX

1. Experimental details

The break-junction technique is realized by a three-point bending mechanism where the substrate is clamped between two counter supports and a mechanically controlled pushing rod on the opposite side. To achieve a vertical movement we use a Faulhaber 2224R024S DC motor operating with rotational speeds in the range of $500\text{--}2000\text{ min}^{-1}$ and a constant gear ratio of 5490:1. The rotation is translated into a vertical displacement by a standardized M4 screw thread, thus, bending the substrate. For the given sample geometry with a reduction factor of $r = 1.22 \times 10^{-5}$ this results in an opening speed of the electrode tips of $0.8\text{--}3\text{ nm/min}$ of Ref. [23].

2. Conductance histograms

Conductance histograms for the six elements under study are depicted in Fig. 8. All measurements were constructed from several hundred opening curves (cf. inset of each histogram for precise numbers) recorded at 4.2 K. To confirm the reproducibility of each conductance measurement, at least, two samples for each element were studied. The histograms show data for one representative sample for each element. The data are binned into ten bins per spin-degenerate conductance quantum $G_0 = 2e^2/h$. For Au, Co, Gd, Ir, Pd, and Pt a bias voltage of 1, 2.5, 3, 10, 5, and 1 mV, respectively, was applied to the sample.

3. Current-voltage characteristics

Figure 9 shows the IV 's (black) of the two Gd contacts of which the noise properties are presented in Fig. 6. The left panel in Fig. 9 corresponds to Figs. 6(a) and 6(b) and the right panel to Figs. 6(c) and 6(d). Any dI/dV (gray) is obtained by the numerical derivative of the current-voltage measurement. Within a bias range of -30 to 30 mV we observe a slight difference regarding the nonlinearity of both IV curves. In particular, the contact on the right shows a rather symmetrical nonlinear trend around zero bias which is more pronounced than in the measurements on the regular contact on the left. Hence, we assume that the intrinsic difference of both contacts, which is discussed in the main article by means of noise measurements, might be also reflected in the degree of IV nonlinearities.

- [1] N. Agraït, A. L. Yeyati, and J. M. van Ruitenbeek, Quantum properties of atomic-sized conductors, *Phys. Rep.* **377**, 81 (2003).
- [2] J. Cuevas and E. Scheer, *Molecular Electronics: An Introduction to Theory and Experiment* (World Scientific, Singapore, 2017), Vol. 15.
- [3] W. Schottky, Über spontane Stromschwankungen in verschiedenen Elektrizitätsleitern, *Ann. Phys.* **362**, 541 (1918).
- [4] Y. Blanter and M. Büttiker, Shot noise in mesoscopic conductors, *Phys. Rep.* **336**, 1 (2000).
- [5] M. Kumar, R. Avriller, A. L. Yeyati, and J. M. van Ruitenbeek, Detection of Vibration-Mode Scattering in Electronic Shot Noise, *Phys. Rev. Lett.* **108**, 146602 (2012).
- [6] H. E. van den Brom and J. M. van Ruitenbeek, Quantum Suppression of Shot Noise in Atom-Size Metallic Contacts, *Phys. Rev. Lett.* **82**, 1526 (1999).

- [7] R. J. Soulen, Jr., J. M. Byers, M. S. Osofky, B. Nadgorny, T. Amborse, S. F. Cheng, P. R. Broussard, C. T. Tanaka, J. Nowak, J. S. Moodera, A. Barry, and J. M. D. Coey, Measuring the spin polarization of a metal with a superconducting point contact, *Science* **282**, 85 (1998).
- [8] M. Häfner, J. K. Viljas, D. Frustaglia, F. Pauly, M. Dreher, P. Nielaba, and J. C. Cuevas, Theoretical study of the conductance of ferromagnetic atomic-sized contacts, *Phys. Rev. B* **77**, 104409 (2008).
- [9] S. Egle, C. Bacca, H.-F. Pernau, M. Huefner, D. Hinzke, U. Nowak, and E. Scheer, Magnetoresistance of atomic-size contacts realized with mechanically controllable break junctions, *Phys. Rev. B* **81**, 134402 (2010).
- [10] M. R. Calvo, J. Fernandez-Rossier, J. J. Palacios, D. Jacob, D. Natelson, and C. Untiedt, The Kondo effect in ferromagnetic atomic contacts, *Nature (London)* **458**, 1150 (2009).
- [11] A. Burtzloff, A. Weismann, M. Brandbyge, and R. Berndt, Shot Noise as a Probe of Spin-Polarized Transport through Single Atoms, *Phys. Rev. Lett.* **114**, 016602 (2015).
- [12] M. Kumar, K. K. V. Sethu, and J. M. van Ruitenbeek, Molecule-assisted ferromagnetic atomic chain formation, *Phys. Rev. B* **91**, 245404 (2015).
- [13] R. Vardimon, M. Matt, P. Nielaba, J. C. Cuevas, and O. Tal, Orbital origin of the electrical conduction in ferromagnetic atomic-size contacts: Insights from shot noise measurements and theoretical simulations, *Phys. Rev. B* **93**, 085439 (2016).
- [14] F. Strigl, C. Espy, M. Bückle, E. Scheer, and T. Pietsch, Emerging magnetic order in platinum atomic contacts and chains, *Nat. Commun.* **6**, 6172 (2015).
- [15] F. Strigl, M. Keller, D. Weber, T. Pietsch, and E. Scheer, Magnetism in Pd: Magnetoconductance and transport spectroscopy of atomic contacts, *Phys. Rev. B* **94**, 144431 (2016).
- [16] M. W. Prestel, M. F. Ritter, A. Di Bernardo, T. Pietsch, and E. Scheer, Tuning the magnetic anisotropy energy of atomic wires, *Phys. Rev. B* **100**, 214439 (2019).
- [17] A. Delin and E. Tosatti, The electronic structure of 4d transition-metal mon-atomic wires, *J. Phys.: Condens. Matter* **16**, 8061 (2004).
- [18] A. Smogunov, A. Dal Corso, A. Delin, R. Weht, and E. Tosatti, Colossal magnetic anisotropy of monatomic free and deposited platinum nanowires, *Nat. Nanotechnol.* **3**, 22 (2008).
- [19] P. Gava, A. Dal Corso, A. Smogunov, and E. Tosatti, Magnetism-induced ballistic conductance changes in palladium nanocontacts, *Eur. Phys. J. B* **75**, 57 (2010).
- [20] A. Thiess, Y. Mokrousov, and S. Heinze, Competing magnetic anisotropies in atomic-scale junctions, *Phys. Rev. B* **81**, 054433 (2010).
- [21] M. Kumar, O. Tal, R. H. M. Smit, A. Smogunov, E. Tosatti, and J. M. van Ruitenbeek, Shot noise and magnetism of Pt atomic chains: Accumulation of points at the boundary, *Phys. Rev. B* **88**, 245431 (2013).
- [22] F. Pauly, M. Dreher, J. K. Viljas, M. Häfner, J. C. Cuevas, and P. Nielaba, Theoretical analysis of the conductance histograms and structural properties of Ag, Pt, and Ni nanocontacts, *Phys. Rev. B* **74**, 235106 (2006).
- [23] J. van Ruitenbeek, A. Alvarez, I. Piñeyro, C. Grahmann, P. Joyez, M. Devoret, D. Esteve, and C. Urbina, Adjustable nanofabricated atomic size contacts, *Rev. Sci. Instrum.* **67**, 108 (1996).
- [24] R. Hoffmann-Vogel, Electromigration and the structure of metallic nanocontacts, *Appl. Phys. Rev.* **4**, 031302 (2017).
- [25] V. Janásek, Ultra low noise high bandwidth transimpedance amplifiers (2015), <http://www.janascard.cz/aHome.html>.
- [26] M. A. Karimi, S. G. Bahoosh, M. Herz, R. Hayakawa, F. Pauly, and E. Scheer, Shot noise of 1,4-benzenedithiol single-molecule junctions, *Nano Lett.* **16**, 1803 (2016).
- [27] A. Mu, O. S. Lumbroso, O. Tal, and D. Segal, Origin of the anomalous electronic shot noise in atomic-scale junctions, *J. Phys. Chem. C* **123**, 23853 (2019).
- [28] E. Scheer, N. Agraït, J. C. Cuevas, A. L. Yeyati, B. Ludoph, A. Martín-Rodero, G. R. Bollinger, J. M. van Ruitenbeek, and C. Urbina, The signature of chemical valence in the electrical conduction through a single-atom contact, *Nature (London)* **394**, 154 (1998).
- [29] E. Scheer, W. Belzig, Y. Naveh, M. H. Devoret, D. Esteve, and C. Urbina, Proximity Effect and Multiple Andreev Reflections in Gold Point Contacts, *Phys. Rev. Lett.* **86**, 284 (2001).
- [30] R. Vardimon, M. Klionsky, and O. Tal, Experimental determination of conduction channels in atomic-scale conductors based on shot noise measurements, *Phys. Rev. B* **88**, 161404(R) (2013).
- [31] R. Ahuja, S. Auluck, B. Johansson, and M. S. S. Brooks, Electronic structure, magnetism, and Fermi surfaces of Gd and Tb, *Phys. Rev. B* **50**, 5147 (1994).
- [32] H. E. Nigh, S. Legvold, and F. H. Spedding, Magnetization and electrical resistivity of gadolinium single crystals, *Phys. Rev.* **132**, 1092 (1963).
- [33] B. Olivera, C. Salgado, J. L. Lado, A. Karimi, V. Henkel, E. Scheer, J. Fernández-Rossier, J. J. Palacios, and C. Untiedt, Electronic transport in gadolinium atomic-size contacts, *Phys. Rev. B* **95**, 075409 (2017).
- [34] O. Berg, Elektrischer Transport durch Nanokontakte von Selten-Erd-Metallen, Ph.D. thesis (KIT, Karlsruhe, Germany, 2014).
- [35] S. Tewari and J. M. van Ruitenbeek, Anomalous nonlinear shot noise at high voltage bias, *Nano Lett.* **18**, 5217 (2018).
- [36] E. C. Stoner, Collective electron ferromagnetism, *Proc. R. Soc. London A* **165**, 372 (1938).
- [37] O. K. Andersen, Electronic structure of the fcc transition metals Ir, Rh, Pt, and Pd, *Phys. Rev. B* **2**, 883 (1970).
- [38] O. K. Andersen, J. Madsen, U. K. Poulsen, O. Jepsen, and J. Kollár, Magnetic ground state properties of transition metals, *Physica B+C* **86**, 249 (1977).
- [39] J. F. Janak, Uniform susceptibilities of metallic elements, *Phys. Rev. B* **16**, 255 (1977).